Al-Azhar Bulletin of Science, Section B, Vol. 33, No. 2 (December) 2022, pp. 45-58
http://doi.10.21608/absb.2022.137705.1184

Al-Azhar Bulletin of Science: Section B

NEW INVESTIGATION OF ASYMMETRIC WALL TEMPERATURE AND FLUID-WALL INTERACTION ON RADIATIVE STEADY MHD FULLY DEVELOPED NATURAL CONVECTION IN VERTICAL MICRO-POROUS–CHANNEL

Hussein A. Soliman*

Department of Basic Science, Engineering Division, International Academy for Engineering and Media Science, 6th October, Egypt
*Corresponding Author: Hussein.AbdAllah.Soliman@iaems.edu.eg

Received: 14 May 2022; Revised: 22 June 2022; Accepted: 04 July 2022; Published: 01 Dec 2022

Abstract

This sort of research might be used to improve the design of micro-pumps and micro heat exchangers. Understanding the fluid flow and heat transfer properties of the buoyancy-induced micro pump and micro heat exchangers in microfluidic and thermal systems is extremely important. In three cases of asymmetric distributions of walls temperature of a vertical micro-porous–channel, the effect of viscous dissipation and heat generation on radiative steady MHD fully developed natural convection flow was investigated analytically using Differential Transform Method (DTM) and numerically using Finite Difference Method (FDM). The velocity slip and temperature jump circumstances are both taken into account since they have opposing impacts on the volume flow rate and the heat transfer rate, respectively. Graphs and tables show the effect of each governing parameter on non-dimensional velocity, temperature, local wall shear stress, and local surface heat flux at the microchannel surfaces. The results obtained were validated by comparison with their peers previously published.

Keywords: Asymmetric wall temperature; Fluid-wall interaction; Micro- porous–channel; Analytical and numerical solution.

1. Introduction

Microchannels have endless uses in life applications. As a result, microfluidics has sparked a lot of scientific interest in recent years. In micro-reactor devices, micro-channel is frequently used for integrated cooling or heating. Therefore, it is one of the main components in MEMS (Micro-electro-mechanical systems), NEMS (Nano-electromechanical systems) and biomedical applications such as drug delivery and DNA sequencing [1]. Micro-channel heatsinks, micro jet impingement cooling, and micro heat pipes are some of the current applications for such devices [3]. Knudsen number Kn is a crucial variable in micro-channel analysis and it's also characterizing the effect of rarefaction , It has been defined as the ratio of molecular mean free path λ to characteristic length a [2-3]. For continuous flows, the Knudsen number is relatively low, where the value of $Kn \in (10^{-2}, 10^{-1})$ a phenomenon known as "slip flow" [2]. Categorization of distinct flow regimes based on Kn studied by [4]. [5,6] looked into the temperature jump situation and discovered that fluid wall contact has a significant role.

The fully developed natural convection in open-ended vertical parallel plate microchannel with asymmetric wall temperature distribution in which the effect of rarefaction and fluid wall interaction studied by [2] and [7-9]. This result is improved by [10] by accounting for suction/injection on the microchannel walls. They came to the conclusion that skin friction and heat transfer rate are both highly influenced by the suction/injection parameter. [11] and [12] looked at the temperature jump condition in another work and discovered that the fluid–wall contact had a significant impact. The same problem was studied by [7] after adding the effect of heat generation to come after him [8] to study the effect of radiation on the same issue. Also, the impact of laser radiation and chemical reaction with electromagnetic field and electroosmotic flow of hybrid non-Newtonian fluid via a sinusoidal channel is investigated [20].

In recent past, [13] conducted a theoretical analysis of fully developed mixed convective heat transfer of water/alumina nanofluid within a vertical microchannel, using the modified Buongiorno's model. For mixed convection, [14] investigated the first-order fully developed mixed convection in a vertical planar microchannel with asymmetric wall temperatures analytically. [14] went on to expand their research to include is flux walls and an annular cross-section produced by two concentric micro tubes. [15] investigated fully developed slip flow mixed convection in vertical micro ducts of two distinct cross-sections, namely polygon, and rectangle, using the circle as a limiting example. Newly, In the presence of viscous dissipation, [16] conducted a theoretical examination of fully developed mixed convection flow in an open-ended vertical parallel plate microchannel. The flow and heat transfer of a squeezed particle fluid with thermal radiation effects between parallel plates studied [19]. Also, [17-18] studied the mathematical modelling and exact solution of steady fully developed mixed convection flow in a vertical micro-porous-annulus.

Due to the rapid growth of novel techniques applied in micro-electro-mechanical systems, manufacturing, material processing operations, space systems, and biomedical applications such as drug delivery, DNA sequencing, and bio-micro-electro-mechanical systems, micro-channel fluid mechanics has attracted significant research interest in recent years. Based on the foregoing, the aim of this study is present a new investigation of asymmetric distributions of walls temperature of a vertical micro- porous–channel with effect of viscous dissipation and heat generation on radiative steady MHD fully developed natural convection flow in different three cases of wall ambient temperature ratio analytically using (DTM) and numerically using (FDM). The present work extends the work of [2] and [7,8].

2. Formulation of the Problem

A fully developed natural convection flow of viscous incompressible and electrically conducting fluid in a vertical parallel plate micro-porous–channel in the presence of viscous dissipation is considered as shown in Fig.1. The distance between two parallel plates is a and temperatures of the hotter and cooler plates are T_1 and T_2 where $T_1 > T_2$. The gravitational acceleration g in the same direction of x – axis and orthogonal to y - axis and B_0 is normally a uniform magnetic field acting on parallel plates. The parameters of thermal radiation and heat generation are taken into account. Fluid is injected into the flow zone through the cold porous plate, and fluid is sucked out of the micro-porous–channel at the same rate through the hot porous plate to conserve the mass of the fluid in the micro-porous–channel. The fluid's physical characteristics are believed to be constant. Using Boussinesq's approximation, the dimensional governing equations of the continuity, momentum and energy can be written as follows [8,9]:

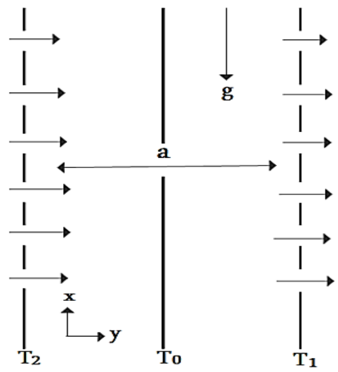

Fig.1. Geometry of the problem.

Continuity equation:

$$\frac{dv}{dy} = 0 \tag{1}$$

Momentum equation:

$$\nu \frac{d^2u}{dy^2} - \frac{\sigma B_0^2}{\rho} u + g\, \beta_T (T - T_0) - \frac{\nu}{K_1} u = 0 \tag{2}$$

Energy equation:

$$\alpha \frac{d^2T}{dy^2} + \frac{Q_0}{\rho c_P}(T - T_0) + \frac{\nu}{c_P}\left[\frac{du}{dy}\right]^2 - \frac{1}{\rho c_p}\frac{\partial q_r}{\partial y} = 0 \tag{3}$$

Where u – horizontally fluid velocity, v -vertically fluid velocity, g - gravitational acceleration, T_1- temperature of hot plate, T_2- temperature of cold plate , B_0 - uniform magnetic field, ρ - fluid density, ν - the kinematic viscosity, σ- fluid electrical conductivity, β_T-thermal expansion coefficient, T- temperature of fluid, T_0-reference temperature, K_1-permeability parameter, α - thermal diffusivity, Q_0 - heat generation parameter, c_p - specific heat at constant pressure and q_r - radiative flux vector , respectively.

The relevant u and T boundary conditions are as follows:

$$\begin{cases} u = \frac{\lambda(2-F_v)}{F_v}\frac{du}{dy}\ , T = T_2 + \frac{2\gamma\lambda(2-F_t)}{P_r F_t(\gamma+1)}\frac{dT}{dy}\ at\ y = 0 \\ u = -\frac{\lambda(2-F_v)}{F_v}\frac{du}{dy}\ , T = T_1 - \frac{2\gamma\lambda(2-F_t)}{P_r F_t(\gamma+1)}\frac{dT}{dy}\ at\ y = 1 \end{cases} \tag{4}$$

Where λ -molecular mean free path, F_v-tangential momentum accommodation coefficient, $\gamma = \frac{c_p}{c_v}$ a ratio of specific heats where c_v-specific heat at constant volume, F_t-tangential thermal accommodation coefficient and P_r-Prandtl number.

For an optically thick fluid, the radiative flow vector may be expressed as [15].

$$q_r = -\frac{4\ \sigma^*}{3\ k^*}\ \frac{\partial T^4}{\partial x}\ , \tag{5}$$

If the difference between T- fluid temperature and T_0- free stream temperature is very little, T^4 may be represented as a Taylor series about T_0, and if the second and higher-order components in the series are ignored, we get:

$$T^4 \cong 4\ T_\infty^3\ T - 3\ T_\infty^4 \tag{6}$$

When applying Eqs.(5-6) in Eq.(3), then:

$$\alpha\left[1 + \frac{16\ \sigma^* T_0^3}{3\ a^* k_T}\right]\frac{d^2T}{dy^2} + \frac{Q_0}{\rho c_P}(T - T_0) + \frac{\nu}{c_P}\left[\frac{du}{dy}\right]^2 = 0 \tag{7}$$

The following non-dimensional variables are introduced as:

$$\eta = \frac{y}{a}\ , \theta = \frac{T - T_0}{T_1 - T_0}\ , f = \frac{\nu u}{g\ \beta_T a^2(T - T_0)}, P_r = \frac{\nu}{\alpha}, \xi = \frac{T_2 - T_0}{T_1 - T_0}\ , \beta_v = \frac{(2-F_v)}{F_v}, \beta_t = \frac{2\gamma\lambda(2-F_t)}{P_r F_t(\gamma+1)}, k_n = \frac{\lambda}{a} \text{ and } l_n = \frac{\beta_t}{\beta_v}.$$

The non-dimensional form of Eqs. (2) and (7) as below:

$$\frac{d^2 f}{d\eta^2} - \left[M + \frac{1}{K}\right] f + \theta = 0 \tag{8}$$

$$\left[1 + \frac{4}{3R_d}\right]\frac{d^2\theta}{d\eta^2} + E_c\left[\frac{df}{d\eta}\right]^2 + H\theta = 0 \tag{9}$$

Where $M = \frac{\sigma B_0^2 a^2}{\rho\nu}$ - magnetic parameter, $K = \frac{K_1}{a^2}$ - permeability parameter, $R_d = \frac{a^* k_T}{4\ \sigma^* T_0^3}$ - radiation parameter, $H = \frac{Q_0 a^2}{k_T}$ - heat generation parameter and $E_c = \frac{\rho g^2 \beta_T^2 a^4 (T - T_0)}{\nu k_T}$ - Eckert number.

In non-dimensional form, the relevant boundary conditions are expressed as:

$$\begin{cases} f = \beta_v k_n \frac{df}{d\eta} \\ \theta = \xi + \beta_v\ k_n\ l_n \frac{d\theta}{d\eta} \end{cases} \quad at\ \ \eta = 0, \tag{10}$$

$$\begin{cases} f = -\beta_v k_n \frac{df}{d\eta} \\ \theta = 1 - \beta_v\ k_n\ l_n \frac{d\theta}{d\eta} \end{cases} \quad at\ \ \eta = 1. \tag{11}$$

Where ξ- Wall ambient temperature, k_n - Knudsen Number, l_n - Fluid wall interaction parameter.

It's now time to compute the physical values that matter most to us, namely the local wall shear stress or skin friction coefficient and the local surface heat flow. Since the shear stress τ_w and the heat flux q_w are defined as:

$$\tau_w = \nu \left[\frac{du}{dy}\right] \tag{12}$$

$$q_w = -\alpha \left[\frac{dT}{dy}\right] \tag{13}$$

In the non-dimensional form, Cf and Nu are defined as:

$$Cf = \frac{\tau_w}{g\ \beta_T a (T - T_0)} \tag{14}$$

$$Nu = \left[1 + \frac{4}{3R_d}\right] \frac{a\, q_w}{\alpha (T - T_0)} \tag{15}$$

After applying non-dimensional variables (10-13) Eqs. (14-15) take the form:

$$Cf = \left[\frac{df}{dy}\right] \tag{16}$$

$$Nu = -\left[1 + \frac{4}{3R_d}\right]\left[\frac{d\theta}{dy}\right] \tag{17}$$

3. Analytical solution

When the (DTM) is used for solving differential equations with the boundary conditions at infinity or problems that have highly nonlinear behavior, the outcomes were diverse solutions. Furthermore, power series are ineffective when the independent variable has large values. To address this problem, the (MDTM) has been created for the analytical solution of differential equations, and it is discussed in this section. For this, the following nonlinear initial value problem is considered.

By Appling differential transformation theorems on equations (8-9), can be obtained the following recursive relations:

$$(\mathrm{k}+1)(\mathrm{k}+2)\mathrm{F}(\mathrm{k}+2) - \left[M + \frac{1}{K}\right]\mathrm{F}(\mathrm{k}) + \Theta(\mathrm{k}) = 0, \tag{18}$$

$$\left[1 + \frac{4}{3R_d}\right](\mathrm{k}+1)(\mathrm{k}+2)\Theta(\mathrm{k}+2) + E_c \sum_{r=0}^{k} (r+1)(\mathrm{k}-\mathrm{r}+1)\mathrm{F}(r+1)\,\mathrm{F}(\mathrm{k}-r+1) + \mathrm{H}\Theta(\mathrm{k}) = 0. \tag{19}$$

Where F (k) and $\Theta(\mathrm{k})$ are the differential transforms of $\mathrm{u}(\eta)$ and $\theta(\eta)$.

We can consider $f\,`(0) = \varepsilon$ and $\theta\,`(0) = \omega$. (20)

Then differential transform for boundary condition (10) and consideration (20) are as follows:

$$\begin{cases} \mathrm{F}(0) = \beta_v k_n\,(\mathrm{k}+1)\mathrm{F}(\mathrm{k}+1) \\ \Theta(0) = \xi + \beta_v k_n\, l_n(\mathrm{k}+1)\Theta(\mathrm{k}+1)\text{'} \end{cases} \tag{21}$$

$$\begin{cases} \mathrm{F}(1) = \varepsilon \\ \Theta(1) = \omega \end{cases}. \tag{22}$$

Moreover, by substituting equations (21-22) into equations (18-19) and by recursive method and boundary condition (11) we calculate other values of $\mathrm{F}(\mathrm{k})$ and $\Theta(\mathrm{K})$.

4. Numerical solution

The coupled system of non-linear ordinary differential equations (8-9) with boundary conditions (10-11) are solved for the flow velocity and temperature using (FDM) with (ParametricNDSolve using Mathematica 12.3). A quasi-linearization technique is applied to replace the non-linear terms. An iterative scheme is used to solve the quasi-linearized system of difference equations.

$$\frac{d^2 f}{d\eta^2} - \left[M + \frac{1}{K}\right] f + \theta = 0 \tag{23}$$

$$\left[1 + \frac{4}{3R_d}\right]\frac{d^2\theta}{d\eta^2} + E_c \left[\frac{d\hat{f}}{d\eta}\right]\left[\frac{df}{d\eta}\right] + H\theta = 0. \tag{24}$$

Where hat notation denotes the iterated terms that convert equation (24) to a linearized one. The domain of answer $(0 < \eta < 1)$ is divided into m subintervals. The linearized system of coupled non-linear ordinary differential equations (23-24) is transformed to system algebraic equations using Taylor's expansions of the dependent variables about central point as:

$$\frac{df_i}{d\eta} = \frac{f_{i+1} - f_{i-1}}{\Delta} + o(\Delta^2) \quad (25)$$

$$\frac{d^2 f_i}{d\eta^2} = \frac{f_{i+1} - 2f_i + f_{i-1}}{\Delta^2} + o(\Delta^2) \quad (26)$$

$$\frac{d^2 \theta_i}{d\eta^2} = \frac{\theta_{i+1} - 2\theta_i + \theta_{i-1}}{\Delta^2} + o(\Delta^2) \quad (27)$$

Where i = 1, 2, 3, …… , $m + 1$ and m the number of subintervals of the finite domain of solution $(0 < \eta < 1)$.

5. Results and discussion

The current parametric investigation was carried out within acceptable limits $0 \leq \beta_v k_n \leq 0.1$ and $0 \leq l_n \leq 10$ and in the continuum and slip flow regimes $(k_n \leq 0.1)$. Study on the slip-flow in three different cases $(\xi = -0.5, \xi = 0 \; and \; \xi = 0.5)$ of asymmetric distributions of plates temperature (at η =0 the cold plate and at η =1 the hot plate) of a vertical micro- porous–channel has been made. The graphs of micro-channel slip velocity f under the effect of various parameters are shown in Figures (2-8). and through it, we made sure that:

- Figure (2) exhibits the action of M on f for different values of ξ. It is clear that, f decreases with an increase in the magnetic parameter M because the Lorentz force associated with the applied magnetic field opposes fluid flow in the transverse direction.
- Figures (3-6) show the micro-channel slip velocity f for several values of H, k_n, K, and R_d under the effect of ξ. It is clear that the fluid velocity f increases with an increase in any parameter of the four parameters but the increase in H and k_n leads to a large slip velocity jump and the rise in K and R_d leads to a small slip velocity jump.
- Figure (7) demonstrate the impact of E_c and ξ on f. It is observed that, With a rise in the E_c, f achieve their stable state and f increases on increasing ξ.
- Figure (8) depicts action of l_n on f. It is evident that, with an increase in l_n, there is an increase in f at η =0 and a decrease in f at η =1 in the two cases of $\xi = -0.5$ and $\xi = 0$. whereas there is an enhancement in f throughout the micro-channel on increasing l_n in the case of $\xi = 0.5$.
- Figures (9-10) displays the influence of H and R_d on θ for three distinct values of ξ. It is noticed that, θ increases with an increase in H and R_d but It should be observed that the increase in H leads to jump on the fluid temperature θ more than jump on the fluid temperature θ by the increase in R_d and it's clear in the case $\xi = 0.5$.
- Figure (11) presents the influence of E_C with effect of ξ on θ. It has been noted that, θ attain their steady state with an increase in Ec and there is an enhancement in θ with an increase in ξ.
- Figure (12) displays the action of l_n on θ under several cases of ξ. It is observed that there is an enhancement in θ at η =0 and a reduction in θ at η =1 on increasing ln in presence of ξ. It should be noted that the present results agree with [1] results.
- Figure (13) displays the impact of k_n on θ under three distinct cases of ξ. It is observed that there is an enhancement in the fluid temperature θ at η =0 and a reduction in θ at η =1 on increasing k_n in the two cases of $\xi = -0.5$ and $\xi = 0$. But in the third case $\xi = 0.5$ θ increases throughout the microchannel with an increase in k_n. It should be noted that the present results agree with [2] results.

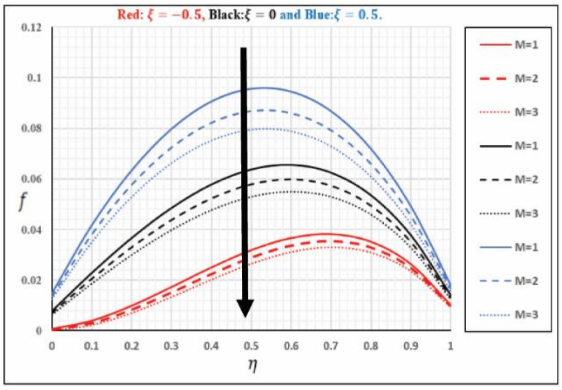

Fig. 2. Action of M on f.

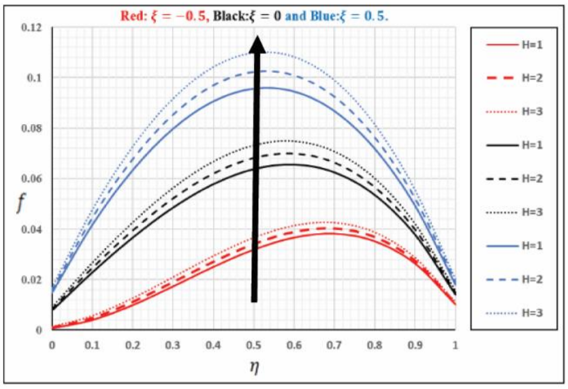

Fig. 3. Action of H on f.

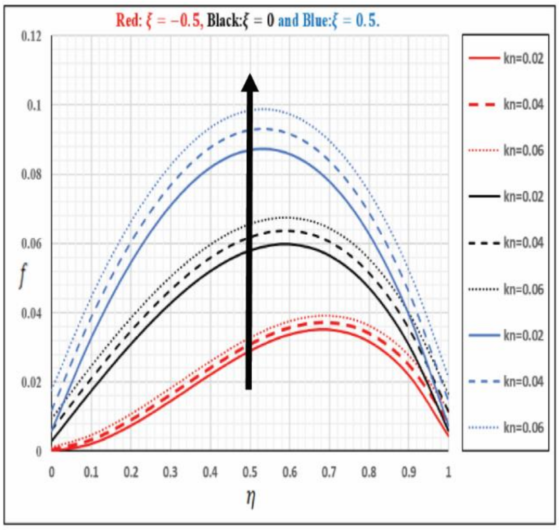

Fig. 4. Action of k_n on f.

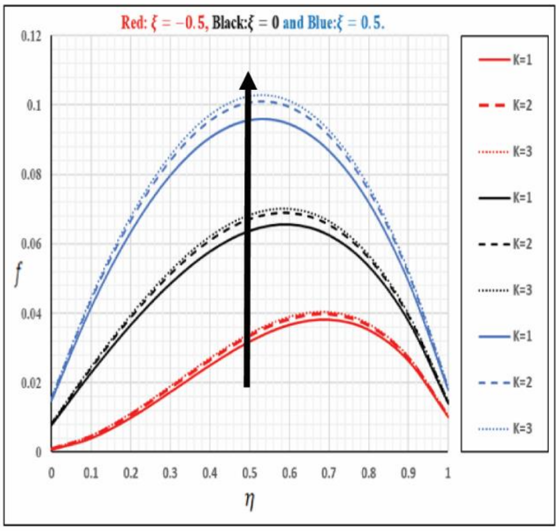

Fig. 5. Impact of K on f.

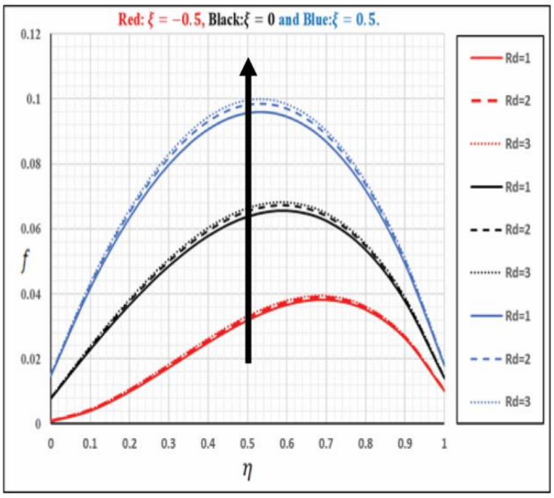

Fig. 6. Action of R_d on f.

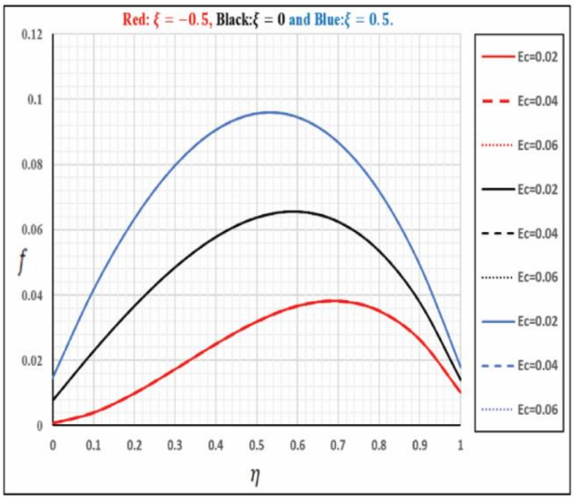

Fig.7. Action of E_c on f

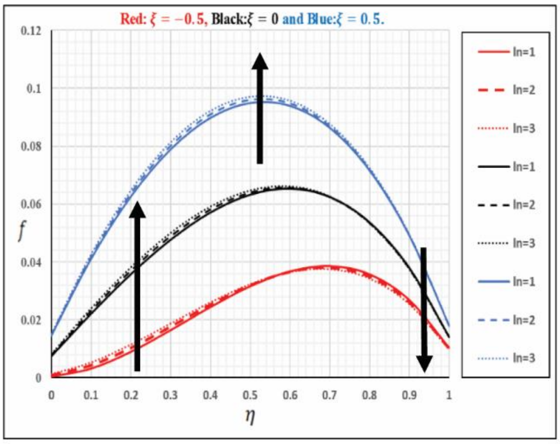

Fig. 8. Impact of fluid l_n on f

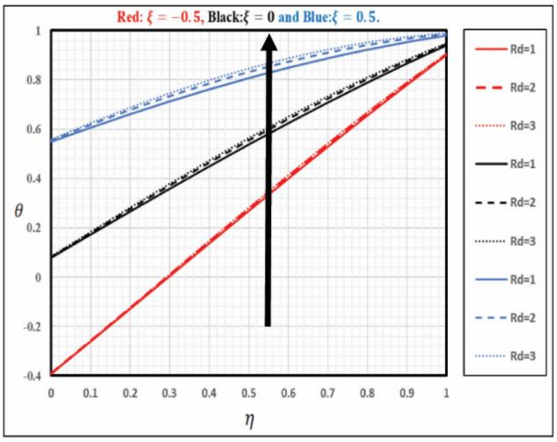

Fig. 9. Action of R_d on θ.

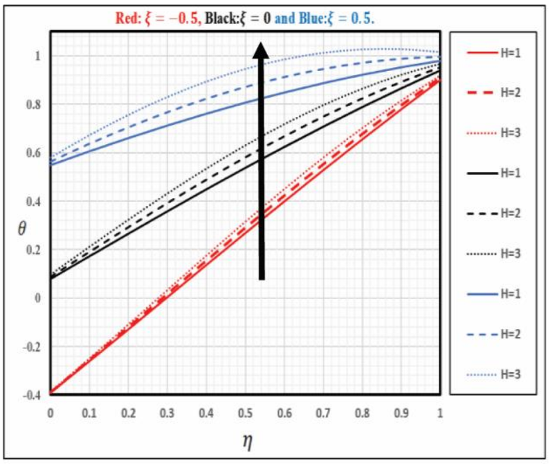

Fig. 10. Action of H on θ.

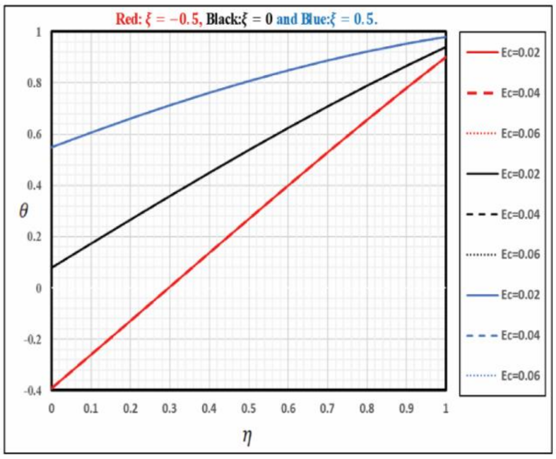

Fig. 11. Action of E_c on θ.

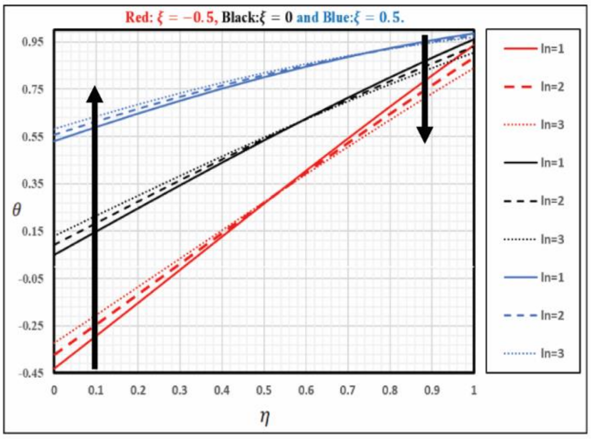

Fig. 12. Action of l_n on θ.

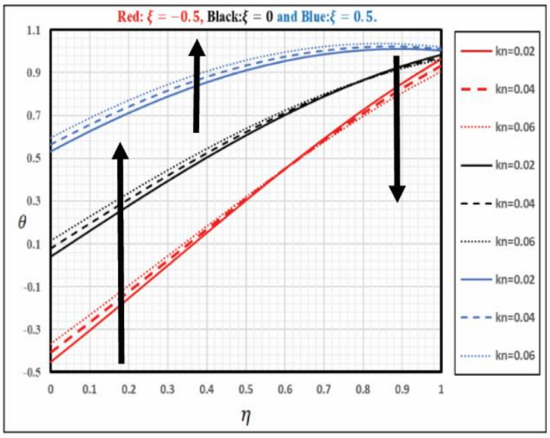

Fig. 13. Action of k_n on θ.

In addition, tables (1-2): Comparison between solution by (DTM) and (FDM) for $f(\eta)$ and $\theta(\eta)$ in three different cases of ξ when $M = 1, K = 1, R_d = 1, E_c = 0.01, H = 1, \beta = 1, k_n = 0.05, \zeta = -0.5$ and $l_n = 1.667$ and equations for $f(\eta)$ and θ (η) distributions will be generated by algebraic computations:

Table 1: Comparison between solution by (DTM) and (FDM) for $f(\eta)$.

η	$f(\eta)$					
	ξ= - 0.5		ξ= 0		ξ= 0.5	
	DTM	FDM	DTM	FDM	DTM	FDM
0	0.0007427	0.0007426	0.0077576	0.0077573	0.0147726	0.0147719
0.1	0.0039830	0.0039819	0.0228510	0.0228422	0.0417191	0.0417034
0.2	0.0099111	0.0099091	0.0366718	0.0366563	0.0634328	0.0634068
0.3	0.0173228	0.0173203	0.0485616	0.0485424	0.0798007	0.0797713
0.4	0.0250384	0.0250355	0.0578347	0.0578150	0.0906314	0.0906053
0.5	0.0318841	0.0318812	0.0637684	0.0637509	0.0956531	0.0956349
0.6	0.0366751	0.0366724	0.0655925	0.0655789	0.0945103	0.0945017
0.7	0.0381965	0.0381943	0.0624774	0.0624683	0.0867586	0.0867583
0.8	0.0351853	0.0351837	0.0535212	0.0535163	0.0718575	0.0718618
0.9	0.0263104	0.0263094	0.0377359	0.0377337	0.0491615	0.0491653
1	0.0101514	0.0101508	0.0140299	0.0140295	0.0179086	0.0179080

Equations for $f(\eta)$ and θ (η) distributions by (DTM):

- ξ= - 0.5
  $f(\eta) = 0.00074272 + 0.01485447\,\eta + 0.19646266\,\eta^2 - 0.212125327\,\eta^3 + 0.025753818\,\eta^4 - 0.016560469\,\eta^5 + 0.00181839\,\eta^6 - 0.00083859\,\eta^7 + 0.000065399\,\eta^8 - 0.000023274\,\eta^9 + 0.0000015569\,\eta^{10}.$
- ξ= 0
  $f(\eta) = 0.007757604 + 0.15515209\,\eta - 0.031576259\,\eta^2 - 0.105586632\,\eta^3 - 0.0038536304\,\eta^4 - 0.0071885631\,\eta^5 - 0.000278161\,\eta^6 - 0.000376521\,\eta^7 - 0.0000095392\,\eta^8 - 0.000010235\,\eta^9 - 1.948153027 \times 10^{-7}\eta^{10}.$
- ξ= 0.5
  $f(\eta) = 0.0147725556 + 0.295451113\,\eta - 0.2596159786\,\eta^2 + 0.0009490742\,\eta^3 - 0.033454151518\,\eta^4 + 0.00217397752\,\eta^5 - 0.00236726402\,\eta^6 + 0.000081889\,\eta^7 - 0.0000831258666\,\eta^8 + 0.000002374499\,\eta^9 - 0.0000018258898\,\eta^{10}.$

Equations for $f(\eta)$ distributions by (FDM):

- ξ= - 0.5
  $f(\eta)$= 0.0027557 η^{10}- 0.013503 η^9+ 0.027199 η^8- 0.029382 η^7+ 0.017957 η^6- 0.020646 η^5+ 0.025545
  η^4- 0.21177 η^3+ 0.19641 η^2+ 0.014846 η + 0.0007426.
- ξ= 0
  $f(\eta)$ = 0.0082672 η^{10}- 0.040234 η^9+ 0.083829 η^8- 0.098049 η^7+ 0.069253 η^6- 0.038015 η^5+ 0.0041106 η^4- 0.10647 η^3 - 0.031478η^2+ 0.15506 η + 0.0077573.
- ξ= 0.5
  $f(\eta)$ = 0.0085428 η^{10}- 0.044505 η^9+ 0.10086 η^8- 0.1302 η^7+ 0.10242 η^6- 0.051201 η^5 - 0.017459 η^4- 0.0013377 η^3- 0.25926 η^2+ 0.29528 η + 0.014772.

Table 2: Comparison between solution by (DTM) and (FDM) for θ(η).

η	$\theta(\eta)$					
	ξ= - 0.5		ξ= 0		ξ= 0.5	
	DTM	FDM	DTM	FDM	DTM	FDM
0	-0.391439	-0.391441	0.078667	0.078662	0.548777	0.548765
0.1	-0.260448	-0.260465	0.172814	0.172596	0.606079	0.605537
0.2	-0.128341	-0.128369	0.266218	0.265887	0.660782	0.660023
0.3	0.004315	0.004280	0.358482	0.358124	0.712652	0.711922
0.4	0.136954	0.136917	0.449209	0.448897	0.761468	0.760944
0.5	0.269005	0.268972	0.538012	0.537798	0.807022	0.806806
0.6	0.399904	0.399878	0.624509	0.624422	0.849118	0.849237
0.7	0.529089	0.529072	0.708331	0.708367	0.887576	0.887974
0.8	0.656008	0.656000	0.789118	0.789237	0.922231	0.922764
0.9	0.780115	0.780114	0.866524	0.866644	0.952934	0.953363
1	0.900880	0.900878	0.940215	0.940208	0.979551	0.979538

Equations for $\theta\ (\eta)$ distributions by (DTM):

- ξ= - 0.5
  $\theta\ (\eta) = -0.39143988 + 1.30246092\ \eta + 0.08387950\ \eta^2 - 0.09304126\ \eta^3 - 0.00304408\ \eta^4 + 0.00210024\ \eta^5 - 0.00002558\ \eta^6 - 0.00000144\ \eta^7 - 0.00000932\ \eta^8 + 0.00000212\ \eta^9 - 7.64184582 \times 10^{-7}\ \eta^{10}$.
- ξ= 0
  $\theta\ (\eta) = 0.07866772 + 0.94382398\ \eta - 0.01690895\ \eta^2 - 0.067402001\ \eta^3 + 0.00063757\ \eta^4 + 0.00143678\ \eta^5 - 0.00002212\ \eta^6 - 0.00001606\ \eta^7 - 0.00000154\ \eta^8 - 5.16567013 \times 10^{-8}\eta^9 - 1.35220286 \times 10^{-7}\eta^{10}$.
- ξ= 0.5
  $\theta\ (\eta) = 0.54877706 + 0.58520778\ \eta - 0.11778213\ \eta^2 - 0.041581402\ \eta^3 + 0.00410961\ \eta^4 + 0.000908607\ \eta^5 - 0.00007947\ \eta^6 - 0.00000718\ \eta^7 - 0.00000192\ \eta^8 + 2.79571489 \times 10^{-7}\eta^9 - 2.111342308 \times 10^{-7}\eta^{10}$.

Equations for θ (η) distributions by (FDM):

- ξ= - 0.5
  $\theta\ (\eta) = 0.29762\ \eta^{10} - 1.4936\ \eta^9 + 3.2267\ \eta^8 - 3.9279\ \eta^7 + 2.9592\ \eta^6 - 1.4219\ \eta^5 + 0.43107\ \eta^4 - 0.1727\ \eta^3 + 0.09189\ \eta^2 + 1.302\ \eta - 0.39144$.
- ξ= 0
  $\theta\ (\eta) = 0.066138\ \eta^{10} - 0.33344\ \eta^9 + 0.71677\ \eta^8 - 0.85731\ \eta^7 + 0.62507\ \eta^6 - 0.28549\ \eta^5 + 0.081402\ \eta^4 - 0.082397\ \eta^3 - 0.010327\ \eta^2 + 0.94114\ \eta + 0.078662$.
- ξ= 0.5.
  $\theta\ (\eta) = 0.26455\ \eta^{10} - 1.3476\ \eta^9 + 2.9489\ \eta^8 - 3.6225\ \eta^7 + 2.7374\ \eta^6 - 1.3101\ \eta^5 + 0.39733\ \eta^4 - 0.12302\ \eta^3 - 0.0921\ \eta^2 + 0.57787\ \eta + 0.54876$.

Moreover, tables (3-13) explain the variation of Cf and Nu in three different cases of ξ at the two plates (cold plate at η =0 and hot plate at η =1.) in symmetric and asymmetric heating under effect different parameters at the standard values M=1, K=1, R_d=1, H=1, E_c= 0.01, k_n=0.05 and l_n=1.667, respectively**.** It is observed that:

1. local wall shear stress or skin friction coefficient Cf:
   - ✓ Decreases at η =0 and increases at η =1 with an increase in M.
   - ✓ Increases at both η =0 and η =1with an increase in k_n and l_n.
   - ✓ An enhancement at η =0 and a reduction at η =1 with an increase in K, R_d, H and E_c.
2. local surface heat flux Nu:
   - ✓ Increases at η =0 and decreases at η =1 with an increase in R_d.
   - ✓ Increases at both η =0 and η =1 with an increase in k_n and l_n.
   - ✓ Decreases at η =0 and increases at η =1 with an increase in H and E_c.

Furthermore, tables (3-14) in the case ξ= 0.5 shows the comparisons with previously published works [8]. It should be highlighted that the current findings are highly accurate and show great agreement.

Table 3: Action of M on Cf.

M	ξ=- 0.5		ξ= 0		Present at ξ= 0.5		ξ= 0.5 [8]	
	η =0	η =1	η =0	η =1	η =0	η =1	η =0	η =1
0.5	0.0186758	-0.209008	0.164241	-0.291129	0.309808	-0.373252	0.3098	-0.3733
1	0.0148545	-0.203014	0.155152	-0.280593	0.295451	-0.358173	0.2954	-0.3582
1.5	0.0114574	-0.197499	0.146951	-0.270981	0.282445	-0.344464	0.2824	-0.3445

Table 4: Action of K on Cf.

K	ξ=- 0.5		ξ= 0		Present ξ= 0.5		ξ= 0.5 [8]	
	η =0	η =1	η =0	η =1	η =0	η =1	η =0	η =1
0.3	0.00177262	-0.180445	0.122731	-0.241881	0.243689	-0.303316	0.2437	-0.3033
0.6	0.0104088	-0.195756	0.144393	-0.267962	0.278378	-0.340167	0.2784	-0.3402
0.9	0.0140652	-0.201749	0.153257	-0.278382	0.292451	-0.355015	0.2924	-0.3551

Table 5: Action of R_d on Cf.

R_d	ξ=- 0.5		ξ= 0		Present at ξ= 0.5		ξ= 0.5 [8]	
	η =0	η =1	η =0	η =1	η =0	η =1	η =0	η =1
1	0.0148545	-0.203014	0.155152	-0.280593	0.295451	-0.358173	0.2954	-0.3582
2	0.0168905	-0.205984	0.159847	-0.285911	0.302806	-0.365839	0.3028	-0.3659
3	0.0180379	-0.207639	0.162481	-0.288883	0.306926	-0.370128	0.3069	-0.3702

Table 6: Action of H on Cf.

H	ξ=- 0.5		ξ= 0		Present at ξ= 0.5		ξ= 0.5 [8]	
	η =0	η =1	η =0	η =1	η =0	η =1	η =0	η =1
1	0.0148545	-0.203014	0.155152	-0.280593	0.295451	-0.358173	0.2954	-0.3582
2	0.0201812	-0.210697	0.167376	-0.294388	0.314573	-0.37808	0.3146	-0.3781
3	0.0263944	-0.219335	0.181419	-0.310047	0.336447	-0.400761	0.3364	-0.4008

Table 7: Action of E_c on Cf.

E_c	ξ=- 0.5		ξ= 0		Present at ξ= 0.5		ξ= 0.5 [8]	
	η =0	η =1	η =0	η =1	η =0	η =1	η =0	η =1
0.02	0.0148555	-0.203015	0.155155	-0.280596	0.295457	-0.358178	0.2955	-0.3583
0.04	0.0148576	-0.203017	0.155160	-0.280601	0.295468	-0.358190	0.2955	-0.3584
0.06	0.0148597	-0.203019	0.155165	-0.280607	0.295479	-0.358202	0.2955	-0.3585

Table 8: Action of K_n on Cf.

k_n	ξ=- 0.5		ξ= 0		Present at ξ= 0.5		ξ= 0.5 [8]	
	η =0	η =1	η =0	η =1	η =0	η =1	η =0	η =1
0.02	0.00101361	-0.219884	0.147945	- 0.293859	0.294877	-0.367836	0.2949	-0.3679
0.04	0.0106122	-0.208243	0.152982	-0.284737	0.295353	-0.361232	0.2953	-0.3613
0.06	0.0187734	-0.198130	0.157122	-0.276694	0.295471	-0.355259	0.2955	-0.3553

Table 9: Action of l_n on Cf.

l_n	ξ=- 0.5		ξ= 0		Present at ξ= 0.5		ξ= 0.5 [8]	
	η =0	η =1	η =0	η =1	η =0	η =1	η =0	η =1
2	0.0177989	-0.200894	0.157665	-0.279729	0.297533	-0.358566	0.2975	-0.3586
4	0.0330821	-0.1907002	0.171247	-0.276327	0.309414	-0.361955	0.3094	-0.3620
6	0.0453742	-0.183739	0.182996	-0.275241	0.320622	-0.366745	0.3207	-0.3668

Table 10: Action of R_d on Nu.

R_d	ξ=- 0.5		ξ= 0		Present at ξ= 0.5		ξ= 0.5 [8]	
	η =0	η =1	η =0	η =1	η =0	η =1	η =0	η =1
1	-3.03908	-2.77479	-2.20226	- 1.67364	-1.36548	-0.572457	-1.3655	-0.5724
2	-2.18459	-1.9141	-1.63674	- 1.09572	-1.08893	-0.277288	-1.0889	-0.2773
3	-1.90037	-1.62641	-1.44957	- 0.901605	-0.998821	-0.176758	-0.9988	-0.1767

Table 11: Action of H on Nu.

H	ξ=- 0.5		ξ= 0		Present at ξ= 0.5		ξ= 0.5 [8]	
	η =0	η =1	η =0	η =1	η =0	η =1	η =0	η =1
1	-3.03908	-2.77479	-2.20226	-1.67364	-1.3654848	-0.572457	-1.3655	-0.5724
2	-3.09198	-2.53125	-2.43516	-1.31364	-1.7783974	-0.0959967	-1.7784	-0.0960
3	-3.16196	-2.26572	-2.7055	-0.912946	-2.2490993	0.439885	-2.2491	0.4399

Table 12: Action of E_c on Nu.

E_c	ξ=- 0.5		ξ= 0		Present at ξ= 0.5		ξ= 0.5 [8]	
	η =0	η =1	η =0	η =1	η =0	η =1	η =0	η =1
0.02	-3.03909	-2.77474	-2.20233	-1.67354	-1.365653	-0.572269	-1.3657	-0.5722
0.04	-3.03914	-2.77466	-2.202467	-1.673352	-1.365989	-0.571893	-1.3660	-0.5718
0.06	-3.03918	-2.77457	-2.202606	-1.673159	-1.366326	-0.571517	-1.3663	-0.5713

Table 13: Action of K_n on Nu.

k_n	ξ=- 0.5		ξ= 0		Present at ξ= 0.5		ξ= 0.5 [8]	
	η =0	η =1	η =0	η =1	η =0	η =1	η =0	η =1
0.02	-3.30096	-3.03962	-2.37487	-1.85217	-1.448833	-0.664677	-1.4489	-0.6646
0.04	-3.12137	-2.85807	-2.25645	-1.72982	-1.391589	-0.601541	-1.3916	-0.6015
0.06	-2.96125	-2.69596	-2.15104	-1.62042	-1.340878	-0.544848	-1.3409	-0.5448

Table 14: Action of l_n on Nu.

l_n	ξ=- 0.5		ξ= 0		Present at ξ= 0.5		ξ= 0.5 [8]	
	η =0	η =1	η =0	η =1	η =0	η =1	η =0	η =1
2	-2.96134	-2.69605	-2.15110	-1.62048	-1.340909	-0.544877	-1.3409	-0.5448
4	-2.57082	-2.29936	-1.89487	-1.35191	-1.218975	-0.404408	-1.2190	-0.4043
6	-2.27659	-1.99868	-1.70304	-1.14714	-1.129535	-0.295550	-1.1295	-0.2954

6. Conclusion

Study on the slip-flow under actions of different parameters in three different cases ($\xi = -0.5, \xi = 0$ and $\xi = 0.5$) of asymmetric distributions of walls temperature of a vertical micro- porous–channel has been made by two different methods of solutions one of them analytically using (DTM) and the other numerically using (FDM). The actions of different parameters M, K, R_d, H, E_c, k_n and l_n on f, θ, Cf, and Nu has been studied graphically and numerically. In particular, results for different parameters are summarized in the next two paragraphs:

- The fluid velocity f:
  - ✓ Increases with an increase in H, k_n, K, and R_d under the effect of ξ.
  - ✓ Decreases with an increase in the magnetic parameter M.
  - ✓ Stable state with an increase in E_c.
  - ✓ Increase at η =0 and a decrease at η =1 with an increase in l_n.
- The fluid temperature θ:
  - ✓ Increases with an increase in H and R_d.
  - ✓ Steady-state with an increase in E_C.
  - ✓ An enhancement at η =0 and a reduction at η =1 on increasing l_n in presence of ξ.
  - ✓ An enhancement in the fluid temperature at η =0 and a reduction at η =1 on increasing k_n in the two cases of $\xi = -0.5$ and $\xi = 0$. But in the third case $\xi = 0.5$ increases throughout the microchannel with an increase in k_n.

Furthermore, Comparisons with previously published works are performed and showed that the present results have high accuracy and are found to be in excellent agreement. The findings of [2] and [7-9] are backed up by this research.

Acknowledgment

Many thanks and appreciation to all the journal's staff for responding quickly to all inquiries regarding publication in the journal and for their great cooperation.

List of abbreviations

2b	Distance between the plates
g	Gravity
T	Temperature
T_1, T_2	Temperatures at left and right plates, respectively
T_m	Mean temperature
c_p	Specific heat at constant pressure
ρ	Fluid density
λ	Molecular mean free path
ξ	Wall ambient temperature
q_r	Radiative heat flux

σ^* Stephan–Boltzmann constant
K Permeability parameter
F_v Tangential momentum accommodation coefficient
F_t Tangential thermal accommodation coefficient
B_0 Uniform magnetic field
γ Ratio of specific heats
ν The kinematic viscosity
σ Fluid electrical conductivity
β_T Thermal expansion coefficient
u Horizontally fluid velocity,
v Vertically fluid velocity
u Velocity of fluid
η Dimensionless variable
f Dimensionless velocity
θ Dimensionless temperature
E_c Eckert number
P_r Prandtl number
H Heat generation parameter
k_n Knudsen Number
H_a^2 Hartman number
M Magnetic parameter
R_d Radiation parameter
l_n Fluid wall interaction parameter
Cf Skin friction coefficient
Nu Nusslet number (local surface heat flux)
DTM Differential transform method
MDTM Multi−step differential transform method
FDM Finite difference method

References

[1] Avci M, Aydin O. Mixed Convection in a Vertical Parallel Plate Microchannel. ASME J. Heat Transfer. 2007; 129(2), pp. 162–166.

[2] Chen COK, Weng HC. Natural convection in a vertical microchannel. 2005; Sep 127(9): 1053-1056.

[3] Jha BK, Aina B, Ajiya AT. MHD natural convection flow in a vertical parallel plate microchannel. Ain Shams Engineering Journal. 2015; 6.1: 289-295.

[4] Chambre PA, Schaaf SA. Flow of rarefied gases. In Flow of Rarefied Gases. Princeton University Press 2017.

[5] Larrode FE, Housiadas C, Drossinos Y. Slip-Flow Heat Transfer in Circular Tubes. Int. J. Heat Mass Transfer. 2000; 43, pp. 2669–2680.

[6] Yu S, Ameel TA. Slip-Flow Heat Transfer in Rectangular Microchannels. Int. J. Heat Mass Transfer. 2001; 44, pp. 4225–4234.

[7] Venkateswarlu M, Prameela M, Makinde OD. Influence of heat generation and viscous dissipation on hydromagnetic fully developed natural convection flow in a vertical micro-channel. Journal of Nanofluids. 2019; 8.7: 1506-1516.

[8] Ponna B, Venkateswarlu M. Influence of Heat Generation and Thermal Radiation on MHD Flow in a Vertical Micro-Porous-Channel in the Presence of Viscous Dissipation. Mapana Journal of Sciences. 2021; 20.2: 27.

[9] Jha BK, Babatunde A. Impact of Viscous Dissipation on Fully Developed Natural Convection Flow in a Vertical Microchannel. Journal of Heat Transfer. 2018; 140.9.

[10] Ha BK, Aina B, Joseph SB. Natural convection flow in a vertical micro-channel with suction/injection. Proceedings of the Institution of Mechanical Engineers, Part E: Journal of Process Mechanical Engineering. 2013; 228.3: 171-180.

[11] Larrode FE, Housiadas C, Drossinos Y. Slip-flow heat transfer in circular tubes. Int J Heat Mass Transfer. 2000; 43:2669–80.

[12] Yu S, Ameel TA. Slip-flow heat transfers in rectangular microchannels. Int J Heat Mass Transfer. 2001; 44:4225–34.

[13] Ganji DD, Malvandi A. Magnetohydrodynamic Mixed Convective Flow of Al2O3–Water Nanofluid Inside a Vertical Microtube. J. Magn. Magn. Mater. 2014; 369, pp. 132–141.

[14] Avci M, Aydin O. Mixed Convection in a Vertical Micro Annulus Between Two concentric Microtubes. ASME J. Heat Transfer. 2009; 131(1), p. 014502.

[15] Sadeghi M, Sadeghi A, Saidi MH. Gaseous Slip Flow Mixed Convection in Vertical Microducts of Constant but Arbitrary Geometry. AIAA J. Thermophys. Heat Transfer. 2014; 28(4), pp. 771–784.

[16] Altunkaya AN, Avci M, Aydin O. Effects of Viscous Dissipation on Mixed Convection in a Vertical Parallel-Plate Microchannel with Asymmetric Uniform Wall Heat Fluxes: The Slip Regime. Int. J. Heat Mass Transfer. 2017; 111, pp. 495–499.

[17] Jha BK, Aina B. Mathematical modelling and exact solution of steady fully developed mixed convection flow in a vertical micro–porous–annulus. J. Afrika Matematika. 2015; Vol. 26, 1199–1213.

[18] Mekheimer KS, Shankar BM, Ramadan SF, Mallik HE, Mohamed MS. On the stability of convection in a non-newtonian vertical fluid layer in the presence of gold nanoparticles: drug agent for thermotherapy. Mathematics, (2021); 9(11), 1302.

[19] Abbas W, Mekheimer KS, Ghazy MM, Moawad AMA. Thermal radiation effects on oscillatory squeeze flow with a particle-fluid suspension. Heat Transfer, (2021); *50*(3), 2129-2149.

[20] Abdelsalam SI, Mekheimer KS, Zaher AZ. Dynamism of a hybrid Casson nanofluid with laser radiation and chemical reaction through sinusoidal channels. Waves in Random and Complex Media. (2022), 1-22.

دراسة جديدة لدرجة حرارة الجدار غير المتكافئة والتفاعل بين السائل الكهرومغناطيسي والجدار على الحمل الحراري الإشعاعي المستقر بالكامل في القناة العمودية الصغيرة المسامية

حسين عبد الله سليمان

قسم العلوم الأساسية- شعبه الهندسة - الأكاديمية الدولية للهندسة وعلوم الاعلام - 6 أكتوبر- مصر

الملخص:

يمكن استخدام هذا النوع من البحث لتحسين تصميم المضخات الدقيقة ومبادلات الحرارة الدقيقة. من المهم للغاية فهم خصائص تدفق السوائل ونقل الحرارة للمضخة الدقيقة التي يسببها الطفو والمبادل الحراري الصغير في الأنظمة الحرارية والموائع الدقيقة. في ثلاث حالات من التوزيعات غير المتكافئة لدرجة حرارة الجدران لقناة عمودية مسامية دقيقة، تم فحص تأثير التبديد اللزج وتوليد الحرارة على تدفق الحمل الحراري الكهرومغناطيسي الطبيعي الثابت الإشعاعي المطوّر بالكامل بشكل تحليلي باستخدام طريقة التحويل التفاضلي (DTM)وعدديًا باستخدام طريقة الفروق المحدودة (FDM). يتم أخذ كل من انزلاق السرعة وظروف قفزة درجة الحرارة في الاعتبار نظرًا لأن لهما تأثيرات متعارضة على معدل تدفق الحجم ومعدل نقل الحرارة، على التوالي. توضح الرسوم البيانية والجداول تأثير كل معلمة تحكم على السرعة غير الأبعاد ودرجة الحرارة وإجهاد قص الجدار المحلي وتدفق حرارة السطح المحلي عند أسطح القناة الدقيقة. تم التحقق من صحة النتائج التي تم الحصول عليها بالمقارنة مع أقرانهم المنشورة سابقا.